Identifying Electronic Modes by Fourier Transform from δ-Kick Time-Evolution TDDFT Calculations

Rajarshi Sinha-Roy, Pablo García-González, Xóchitl López Lozano, Robert Whetten, Hans-Christian Weissker

Identifying Electronic Modes by Fourier Transform from δ-Kick Time-Evolution TDDFT Calculations

Rajarshi Sinha-Roy,[*,†,‡,§] Pablo García-González,[‡,§] Xóchitl López Lozano,[¶] Robert L. Whetten,[¶] and Hans-Christian Weissker[*,†,§]

†*Centre Interdisciplinaire de Nanoscience de Marseille (CINaM), Aix-Marseille University, 13288 Marseille, France*

‡*Departamento de Física Teórica de la Materia Condensada and Condensed Matter Physics Center (IFIMAC), Universidad Autónoma de Madrid, E-28049 Madrid, Spain*

¶*Department of Physics & Astronomy, The University of Texas at San Antonio, One UTSA circle, 78249-0697 San Antonio, TX., USA*

§*European Theoretical Spectroscopy Facility (ETSF)*

E-mail: sinharoy@cinam.univ-mrs.fr; weissker@cinam.univ-mrs.fr

Abstract

Time-Dependent Density-Functional Theory (TDDFT) is widely used for calculating electron excitations in clusters and large molecules. For optical excitations, TDDFT is customarily applied in two distinct approaches: transition-based linear-response TDDFT (LR-TDDFT), and the real-time formalism (RT-TDDFT). The latter does not require the calculation of empty electron orbitals, which is specially advantageous when dealing with large systems. However, RT-TDDFT does not provide direct information on the nature of the excitations, unlike LR-TDDFT where the transition densities and the decomposition of the actual excitations in terms of independent-particle Kohn-Sham transitions are naturally obtained. In the present work, we show that the transition densities of the optically allowed transitions can be efficiently extracted from a single δ-kick time-evolution calculation. We assess the results by comparison with the corresponding LR-TDDFT ones and also with the induced densities arising from RT-TDDFT simulations of the excitation process.

Keywords

Real-time TDDFT, *ab initio*, δ-kick time-evolution, induced density, Fourier transform, dynamical screening, metal clusters, surface-plasmon resonances

Introduction

The study of electronic excitations in molecules and small clusters necessarily employs quantum-mechanical methods. In particular, the description of "quantum-sized" metal clusters takes an intermediate position: for high-level quantum-chemical methods like configuration interaction[1,2] or the coupled-cluster method, which have been used for very small clusters,[3,4] the sizes are too big. By contrast, classical or semiclassical descriptions, ranging from local electrodynamics (Mie theory[5] and extensions thereof) to quantum-corrected mod-

els[6] and hydrodynamic approximations[7–13] cannot, or only partially, represent the quantum effects that need to be accounted for.

In recent years, and in particular for a variety of intermediate-sized metal clusters and large molecules, Time-Dependent Density-Functional Theory (TDDFT)[14] has become the workhorse of computational studies in it's *atomistic* form where the electron-ion interaction is described using either pseudopotentials or localized bases. For instance, localized surface-plasmon resonances (LSPR) which, in the classical picture, correspond to collective oscillations of the quasi-free conduction electrons in a metal cluster,[15] have been treated in a number of recent studies (see, for instance, Refs. 16–23). However, the TDDFT calculations are not restricted to the description of the LSPR. They account for the atomic structure of the clusters, thus going beyond simplistic jellium-based modelling of the clusters.[24–26] In addition, the proper description of the interaction with the *d*-electron excitations[27,28] and with the ligands of wet-chemically produced clusters[29–34] are important issues which are currently debated in the literature.

In practical TDDFT calculations, different approximations are available in order to calculate the electronic response to an external perturbation like a laser field. For instance, the optical linear response is often evaluated using the linear-response TDDFT (LR-TDDFT) approach, in particular using the so-called Casida equation.[35] Such a formalism gives access not only to the absorption spectrum of the studied system, but also to the transition densities that correspond to a particular excitation. A spatial representation of these transition densities provides invaluable insights into the nature of the response of the electronic system. One obtains likewise the decomposition of the excitations in terms of transitions between independent-particle Kohn-Sham[36] (KS) states. However, LR-TDDFT methods have a drawback in practical calculations: a large number of unoccupied (virtual) orbitals and the corresponding transitions between these occupied and unoccupied orbitals have to be obtained. In addition, the number of unoccupied states determines the size of the matrix equations that have to be solved to get the absorption spectrum. Consequently, these

transition-based methods become numerically very demanding for large systems.

By contrast, the real-time formalism of Time-Dependent Density-Functional Theory (RT-TDDFT) relies solely on the explicit time evolution of the occupied Kohn-Sham orbitals under a particular perturbation, which renders it numerically more easily tractable for large systems. Since perturbative expansions are not used, there is no need to calculate unoccupied KS orbitals, thus circumventing the above-mentioned limitation of LR-TDDFT methods. Customarily (Yabana and Bertsch method),[37,38] optical absorption spectra are obtained from a single time-propagation using a Dirac-delta (δ-kick) at $t = 0$, which equally excites all the optically allowed transtions. After the δ-kick perturbation, the system evolves without further perturbation, the time-dependent dipole moment of the system is recorded, and its Fourier transform provides the absorption spectrum.

A clear disadvantage of the RT-TDDFT approach is that, normally, no direct information on the excitations involved in a particular spectral feature is obtained. The results are, therefore, more difficult to interpret than those from LR-TDDFT calculations. This could be remedied by projecting the time-dependent KS wavefunctions onto the ground-state KS wavefunctions, both occupied and empty. This has been done, for instance, for high-symmetry jellium systems,[39] but it is a time-consuming procedure. Likewise, a decomposition of the time-propagated Kohn-Sham *density matrix* obtained in real space has been reported to give transition contributions from different states, as well as the full and partial induced densities.[40]

The availability of the density induced by the δ-kick perturbation, $\rho(\mathbf{r}, t)$, has been used to allay the problem of missing information. In earlier work, some of the present authors have used $\rho(\mathbf{r}, t)$ to discuss features like the LSPR in gold and silver clusters.[41–43] However, this is really useful only when one mode dominates the response of the system and a refined discussion of smaller details is not needed. Quasi-monochromatic laser excitation can likewise be used to study the electronic density modes for a narrow range of energies.[16,44–46] Finally, Fourier-transformed time-dependent densities have been used in the discussion of plasmon

excitations, but restricted to simple low-dimensional Na systems[47] or, by using simplified orbital-free TDDFT, to compact Na clusters.[48]

In the present work, we show that a "standard" time-evolution calculation in the spirit of Yabana and Bertsch can be used to determine accurately the spatial contributions to individual spectral features *at all energies*. In other words, the mapping to electronic modes based on the Fourier transform of the time-dependent induced density provides an efficient, reliable and robust numerical determination of the transtion densities, and not only to the corresponding frequency-dependent dipole moment. We perform a Fourier transform of the time-dependent induced density at each space point to calculate the Fourier coefficients that contribute at any energy of interest. This procedure is applied to simple- and noble-metal structures (Na and Ag, respectively), and assessed by comparing with results obtained in LR-TDDFT or with the transition densities inferred from quasi-monochromatic laser excitations.

Theoretical Background and Methods

Theoretical background:

According to the Yabana and Bertsch formalism,[37,38] the optical response of a finite system under the quasistatic and dipole approximations can be evaluated as follows. Starting from the ground state, at $t = 0$ the electron system is perturbed by a δ-kick electric field polarized along the $\mathbf{u}$ direction

$$\mathbf{E}(\mathbf{r}, t) = K_0 \delta(t) \mathbf{u} = \frac{1}{\pi} \int_0^{+\infty} K_0 \cos(\omega t) \mathbf{u} \, d\omega \; . \tag{1}$$

Thus, the perturbation (1) is the linear superposition of homogeneous monochomatric electric fields covering all possible frequencies. This perturbation leads to an instantaneous transfer of momentum to the system, which evolves freely for $t > 0$. For an electron system which, without loss of generality, has a discrete energy spectrum $E_0 < E_1 \leq E_2 \leq E_3 \leq ...$, and such that the wavefunctions of all the stationary states $|\Psi_j\rangle$ are real, the δ-kick-induced density

for $t > 0$ is

$$\delta\rho(\mathbf{r},t) = -K_0 \sum_{j=1}^{\infty} c_j(\mathbf{r}) \sin(\omega_j t)\,, \tag{2}$$

as long as K_0 is small enough to ensure that the response remain in the linear regime. In Eq. (2), $\omega_j = (E_j - E_0)/\hbar$ are the excitation frequencies, and $c_j(\mathbf{r})$ are the transition densities defined as

$$c_j(\mathbf{r}) = \frac{2e}{\hbar}\mathbf{u} \cdot \int \mathbf{r}' \langle\Psi_0|\hat{\rho}(\mathbf{r})|\Psi_j\rangle\langle\Psi_j|\hat{\rho}(\mathbf{r}')|\Psi_0\rangle d\mathbf{r}'\,, \tag{3}$$

$\hat{\rho}(\mathbf{r})$ being the one-electron density operator. The optical absorption cross-section for $\mathbf{u}$-polarized E-fields will then be given by

$$\begin{aligned} \sigma_{\mathbf{u}}(\omega) &= \frac{\omega e}{c\epsilon_0} \sum_{j=1}^{\infty} \delta(\omega - \omega_j) \int (\mathbf{u}\cdot\mathbf{r}) c_j(\mathbf{r}) d\mathbf{r} \\ &= -\frac{\omega e}{\pi K_0 c \epsilon_0} \mathbf{u} \cdot \Im \int_0^{+\infty} e^{(\mathrm{i}\omega - \eta)t} \left(\int \mathbf{r}\delta\rho(\mathbf{r},t) d\mathbf{r} \right) dt\,, \end{aligned} \tag{4}$$

η being a positive infinitesimal. Thus, the calculation of the absorption spectrum does not require the knowledge of the transition densities, but just of the time-dependent dipole induced by the δ-kick perturbation.

However, the transition densities are needed to characterize optical modes, which can be illustrated by contribution maps, animations or snapshots at different times within the period of oscillation $T_i = 2\pi/\omega_i$. The induced density by each monochromatic component $K_0 \cos(\omega t)\mathbf{u}$ of the perturbing field (1) can be evaluated from the Fourier tranform of $\delta\rho(\mathbf{r},t)$,

$$\delta\rho(\mathbf{r},t,\omega) = K_0 \mathscr{R}(\mathbf{r},t,\omega) = K_0[a(\mathbf{r},\omega)\cos(\omega t) + b(\mathbf{r},\omega)\sin(\omega t)]\,, \tag{5}$$

where a and b are the cosine and sine Fourier transforms of $\delta\rho(\mathbf{r},t)/K_0$, respectively:

$$a(\mathbf{r},\omega) = \frac{1}{K_0} \int_0^{+\infty} \delta\rho(\mathbf{r},t)\cos(\omega t)\mathrm{e}^{-\eta t} dt\,, \tag{6}$$

$$b(\mathbf{r},\omega) = \frac{1}{K_0}\int_0^{+\infty} \delta\rho(\mathbf{r},t)\sin(\omega t)\mathrm{e}^{-\eta t}dt\,. \tag{7}$$

Hence,

$$\mathscr{S}(\mathbf{r},\omega) = \sqrt{a^2(\mathbf{r},\omega)+b^2(\mathbf{r},\omega)}\,, \tag{8}$$

shows the region in space that contributes to the induced density at that frequency.

In terms of the transition densities $c_j(\mathbf{r})$, the Fourier coefficients a and b are given by the known expressions

$$a(\mathbf{r},\omega) = \sum_{j=1}^{\infty} \mathrm{P.P.}\frac{2\omega_j}{\omega^2-\omega_j^2}c_j(\mathbf{r})\,, \tag{9}$$

$$b(\mathbf{r},\omega) = -\pi\sum_{j=1}^{\infty}\delta(\omega-\omega_j)c_j(\mathbf{r})\,, \tag{10}$$

P.P. being the principal part. Hence, if ω equals one of the excitation frequencies ω_i then $\mathscr{R}(\mathbf{r},t,\omega_i)$ will be the corresponding time-dependent transition density. The cosine coefficient $a(\mathbf{r},\omega_i)$ is a regular function which contains contributions from all the remaining excitations with a relative weight of the order $1/(\omega_i-\omega_j)$. Conversely, the sine coefficient $b(\mathbf{r},\omega_i)$ is singular and just proportional to $c_i(\mathbf{r})$. Therefore, the oscillation in phase with the external field can be neglected and the mode is simply $\mathscr{R}(\mathbf{r},t,\omega_i) = -\lim_{\eta\to 0}\eta^{-1}c_i(\mathbf{r})\sin(\omega_i t)$.

Methods: In the TDDFT formalism, the action of the δ-kick perturbation is equivalent to the multiplication of the DFT ground-state occupied KS orbitals $\psi_n^0(\mathbf{r})$ by a position-dependent phase factor $\exp(\mathrm{i}eK_0\mathbf{r}\cdot\mathbf{u}/\hbar)$ at $t=0^+$. Then, the time-dependent occupied KS orbitals $\psi_n(\mathbf{r},t)$ corresponding to the free evolution of the actual electron system are evaluated self-consistently at every time step. As a consequence, the induced electron density is given by

$$\delta\rho(\mathbf{r},t) = \rho(\mathbf{r},t)-\rho_0(\mathbf{r}) = \sum_n^{\mathrm{occ}}(|\psi_n(\mathbf{r},t)|^2-|\psi_n^0(\mathbf{r})|^2), \tag{11}$$

where $\rho_0(\mathbf{r}) = \sum_n^{\mathrm{occ}}|\psi_n^0(\mathbf{r})|^2 = \sum_n^{\mathrm{occ}}|\psi_n(\mathbf{r},0)|^2$ is the ground-state density. Ground-state and time-dependent densities are obtained, respectively, as output from a ground-state DFT

and a RT-TDDFT simulation in the real-space code `octopus`.[49–51] We use norm-conserving Troullier-Martins pseudopotentials[52] and the GGA-PBE approximation[53] to the exchange-correlation functional. The simulation domain is made up by the superposition of spheres around the ions. A grid spacing of 0.18 Å and radius 5.0 Å are used for Ag systems. A grid spacing of 0.3 Å and radius 7.0 Å are used for Na systems. For the time evolution, a time step of 0.0024 $\hbar$/eV and 0.003 $\hbar$/eV are used, respectively, for Ag and Na systems. For our Fourier transforms, a much larger time-step is sufficient: the time-dependent densities are written out for every 50th time step for Na systems and for every 10th time step for Ag systems, respectively. The time propagation is carried out up to $t = T_{\max} \sim 25$ fs. We have then performed the corresponding Fourier transforms to obtain the absorption spectrum (Eq. 4) and the reconstructed modes (Eq. 5, 6 and 7). Frequency dependences are smoothed out by using a finite frequency $\gamma = 0.1$ eV instead of the infinitesimal value η, which also serves to account for non-electronic dissipation mechanism in an approximate manner. Thus, the reconstructed mode (5) actually corresponds to the driven induced density by the quasi-monochromatic laser pulse $E_0 \exp(-\gamma|t|)\cos(\omega t)\mathbf{u}$ at times $|t| \ll \gamma^{-1}$.

For comparison, likewise within the framework of RT-TDDFT simulations, we simulate the actual dynamics due to the excitation by a quasi-monochromatic laser field. In this case, the perturbation corresponds to a time-dependent homogeneous electric field of the form

$$\mathbf{E}(t) = \begin{cases} E_0 \sin(\omega t) \cos\left(\dfrac{t}{T_{\mathrm{e}}} - \dfrac{\pi}{2}\right) \mathbf{u} & \text{if } 0 \leq t \leq T_{\mathrm{e}} \\ \mathbf{0} \quad \text{otherwise} , \end{cases} \tag{12}$$

where E_0 is the amplitude, $\mathbf{u}$ is the polarization, ω is the mean frequency of the laser pulse; T_{e} is half the time period of the envelope of the laser pulse. E_0 is chosen to be $E_0 = 10^{-2}$ eV/Å, which is weak enough to remain in the linear regime but strong enough to ensure that the result is not drowned in numerical "noise". The length of the envelope of the laser pulse is chosen to be such that it can accommodate 10 oscillations of the laser field. The laser

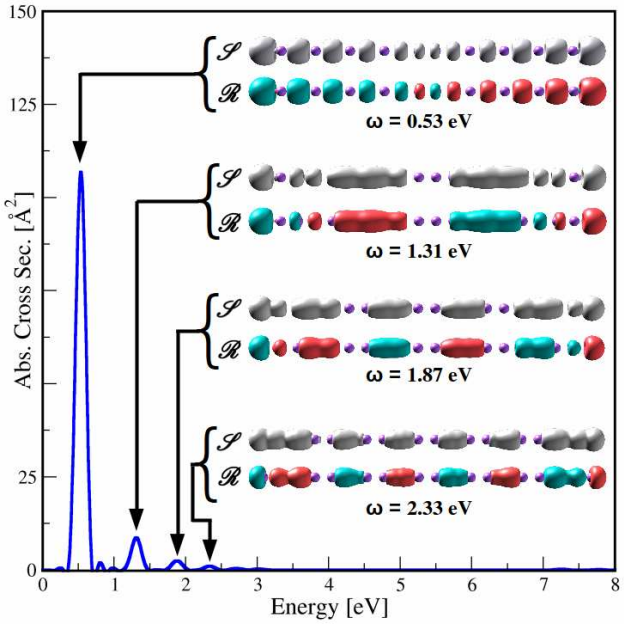

Figure 1: **Absorption spectrum of Na_{20} and induced densities from a δ-kick RT-TDDFT calculation.** Reconstructed modes $\mathscr{R}(\mathbf{r},\ t = T_i/4, \omega_i)$, where $T_i = 2\pi/\omega_i$ is the oscillation period, along with the modulus $\mathscr{S}(\mathbf{r}, \omega_i)$ according to Eq. 8 for the different excitations. The iso values for all the isosurfaces are the same.

pulse is switched on only for $0 \leq t \leq T_e$, the system thereafter evolves freely. Such a free evolution corresponds to superposition of those oscillatory modes within a frequency range centered at the mean frequency of the quasi-monochromatic laser pulse.

Well-separated excitations: The example of simple-metal chains

As a first illustration, we analyze the modes excited in a linear atomic chain of 20 Na atoms by an incident laser pulse polarized along the direction of the chain. In this case, the absorption spectrum is dominated by a series of well-defined highly renormalized electron-hole excitations, each one corresponding to a confined oscillatory collective mode which resemble different harmonics in a stretched string.[54]

Fig. 1 shows the optical absorption for a Na_{20} linear chain calculated by a δ-kick RT-

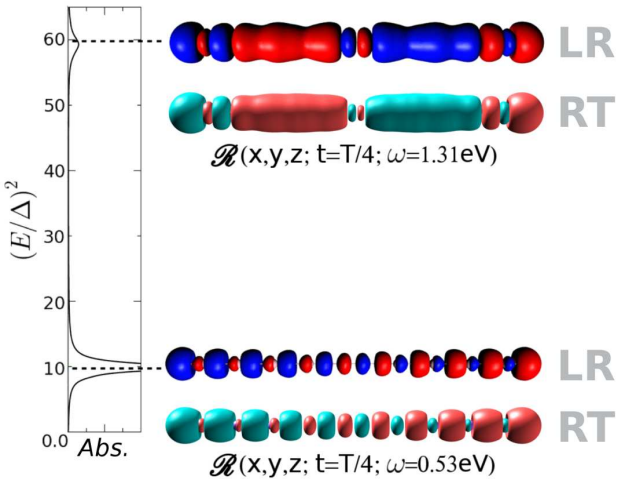

Figure 2: **Comparison of modes from RT- and LR-TDDFT calculations for a Na_{20} linear chain.** The reconstructed modes $\mathscr{R}(\mathrm{r},\ t = T_i/4, \omega_i)$ are compared with the transition densities at the respective energies calculated by Bernadotte *et al.*[54] using LR-TDDFT. The Δ in the energy-axis of the spectrum corresponds to the HOMO-LUMO gap of 0.17 eV.[54] The iso-surface for the modes are adjusted to allow for a direct comparision with the LR-TDDFT ones.

TDDFT calculation. As anticipated, the spectrum is dominated by four distinct absorption peaks of decreasing intensity at energies 0.53 eV, 1.31 eV, 1.87 eV, and 2.33 eV. Fig. 1 also shows the spatial distribution of the modulus $\mathscr{S}(\mathbf{r}, \omega_i)$ of the reconstructed modes as well as snapshots of $\mathscr{R}(\mathbf{r}, t, \omega_i)$ at $t = T_i/4 = \pi/(2\omega_i)$, that is, when the mode is equal to $b(\mathbf{r}, \omega_i)$. As can be observed, the shapes of $\mathscr{S}(\mathbf{r}, \omega_i)$ and $\mathscr{R}(\mathbf{r}, T_i/4, \omega_i)$ are practically the same, which is the expected behavior for well-defined excitations (cf., equations 9 and 10 and their discussion).

In order to asses the reliability of the method, the reconstructed modes for the first two peaks at 0.53 eV and 1.31 eV are compared in Fig. 2 with the corresponding transition densities $c_i(\mathbf{r})$ obtained from the LR-TDDFT approach by Bernadotte *et al.*[54] The excellent agreement confirms that the Fourier-transform-based extraction of information for individual excitations works well, despite the relatively large damping frequency $\gamma = 0.1\, eV$ used in the numerical evaluation of the Fourier transforms.

This accuracy and reliability of the reconstructed modes can be easily understood. If

a non-infinitesimal γ were used to evaluate the Fourier transforms (7) and (8), the real functions $a(\mathbf{r},\omega)$ and $b(\mathbf{r},\omega)$ would be given exactly by

$$a(\mathbf{r},\omega) = \sum_{j=1}^{\infty} \left(\frac{\omega-\omega_j}{(\omega-\omega_j)^2+\gamma^2} - \frac{\omega+\omega_j}{(\omega+\omega_j)^2+\gamma^2} \right) c_j(\mathbf{r})\,, \tag{13}$$

$$b(\mathbf{r},\omega) = \sum_{j=1}^{\infty} \left(\frac{\gamma}{(\omega+\omega_j)^2+\gamma^2} - \frac{\gamma}{(\omega-\omega_j)^2+\gamma^2} \right) c_j(\mathbf{r})\,. \tag{14}$$

As long as γ is small enough to guarantee that there are no further strong excitations within a region of width $\sim 2\gamma$ around ω_i, the calculated sine coefficient (14) will be $b(\mathbf{r},\omega_i) \simeq -(1/\gamma)c_i(\mathbf{r})$. By contrast, the relative contributions by nearby excitations to the cosine coefficient (13) depend quite sensitively on γ, so the shape of the calculated $a(\mathbf{r},\omega_i)$ does depend on the specific value of γ. The reconstructed mode $\mathscr{R}(\mathbf{r},t,\omega_i)$ will acquire a small but non-negligible term $a(\mathrm{r},\omega_i)\cos(\omega_i t)$, which corresponds to an excitation with a finite lifetime, but the term $b(\mathbf{r},\omega_i)\sin(\omega_i t) = \mathscr{R}(\mathbf{r},t=T_i/4,\omega_i)$, which is the one that is naturally associated to the excitation, will be exact up to an overall scaling factor.

Modes in noble-metal nanorods: Ag_{37}

Noble-metal clusters and nanostructures are more complex because here, in addition to the quasi-free metal s electrons, a filled shell of d electrons is present which in silver starts about 4 eV below the Fermi energy, in gold and copper at around 2 eV. For the present work, we consider pentagonal noble-metal nanorods which have been analyzed in a number of studies before.[43,44,55,56] They show, in particular, a strong LSPR mode for excitations along the rod axis, the energy of which is strongly red-shifted with increasing aspect ratio. We emphasize that the treatment of noble-metal clusters is a much more stringent test for the Fourier-transform method to reconstruct optical modes due to the different length scales of oscillation for s and d electrons.

In Fig. 3, the δ-kick spectrum of Ag_{37} excited along its axis and the distributions $\mathscr{S}(\mathbf{r},\omega_i)$

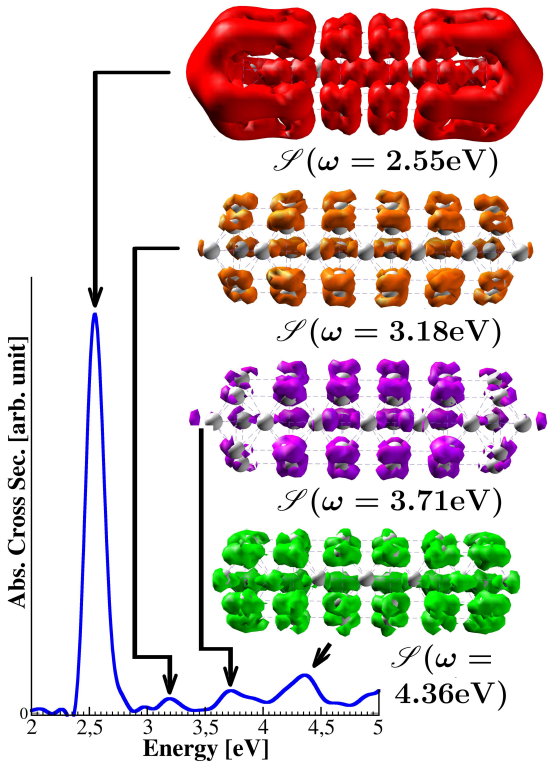

Figure 3: **RT-TDDFT absorption spectrum of Ag_{37} and reconstructed modes at some energies of interest.** The regions ($\mathscr{S}(\mathbf{r}, \omega_i)$) where the induced densities of the modes are large are shown in different colors for the same iso value. The incident E-field is polarized along the main rod axis.

corresponding to different peaks in the spectrum are shown, all for the same isosurface value. The distribution $\mathscr{S}$ at the strong peak at 2.55 eV, which corresponds to the LSPR, reveals that the primary contribution in the formation of the mode comes from the surface of the rod and, in particular, from its ends.[44] By contrast, the reconstructed modes corresponding to the less intense peaks at higher energies (3.18 eV, 3.71 eV, and 4.36 eV), are primarily localized around the silver atoms, suggesting strong contributions from the localized d-electrons. This is consistent with the fact that this part of the spectrum is expected to be dominated by a quasi-continuum of "interband transitions".[57–59]

Fig. 4 shows the Fourier coefficients, $a(\mathbf{r}, \omega)$ and $b(\mathbf{r}, \omega)$, at the LSPR frequency $\omega_{\text{sp}} = 2.55$ eV and at $\omega_{\text{int}} = 3.18$ eV. For the former, although the cosine coefficient is not negligible, the main contribution to the reconstructed mode comes from the excitation

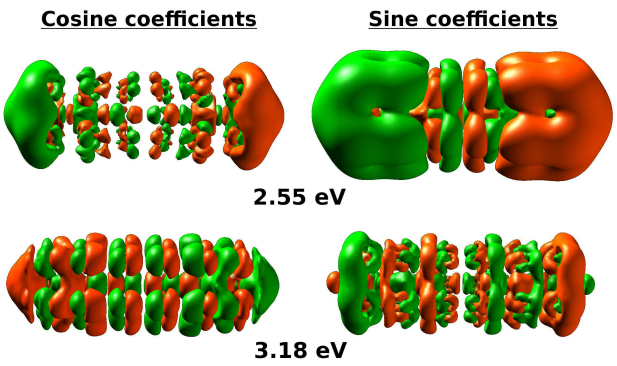

Figure 4: **Cosine and sine coefficients for the reconstructed modes of Ag_{37}.** The coefficients $a(\mathbf{r},\omega)$ (left column) and $b(\mathbf{r},\omega)$ (right column) are shown for two different energies, $\omega_{\rm sp} = 2.55$ eV and $\omega_{\rm int} = 3.18$ eV, corresponding to the localized surface plasmon and to "interband" d-electron transitions, respectively. All isosurfaces are shown for the same value.

part $b(\mathbf{r},\omega_{\rm sp})\sin(\omega_{\rm sp}t)$, a fact that is corroborated by the similarity between the shapes of $\mathscr{S}(\mathbf{r},\omega_{\rm sp})$ and $|b(\mathbf{r},\omega_{\rm sp})|$. In full agreement with the analysis made in the previous section (cf., Eq. 13 and 14), the spectral feature at $\omega_{\rm sp}$ is expected to be dominated by a single excitation with transition density $c_{\rm sp}(\mathbf{r}) \simeq -\gamma b(\mathbf{r},\omega_{\rm sp})$. Consequently, $a(\mathbf{r},\omega_{\rm sp}) \simeq -c_{\rm sp}(\mathbf{r})/(2\omega_{\rm sp})$ at the edges of the rod, but the transition densities of weaker s-electron excitations and of higher-energy d-electron excitations also contribute to the cosine coefficient, the effect from the latter being stronger around each atom. It is worth mentioning that well-defined contributions around the atoms also appear in $b(\mathbf{r},\omega_{\rm sp})$ (that is, in the transition density $c_{\rm sp}(\mathbf{r})$), but with a polarization opposite to the dominating surface mode. They are the signatures of the well-known dynamical screening of the LSPR by d electrons,[41,58,59] which manifests itself in a d-electron oscillation in response to the field created by the dominating collective oscillation of the s-electrons. Regarding the spectral peak at $\omega_{\rm int} = 3.18$ eV, the sine and cosine coefficients contribute almost equally to the reconstructed mode, so none of them resembles the corresponding $\mathscr{S}(\mathbf{r},\omega_{\rm int})$. This indicates that the spectral feature centered at 3.18 eV results from a convolution of several energetically close d-electron excitations. As shown in the Supplementary Information (SI), these d-electron excitations can be spectrally

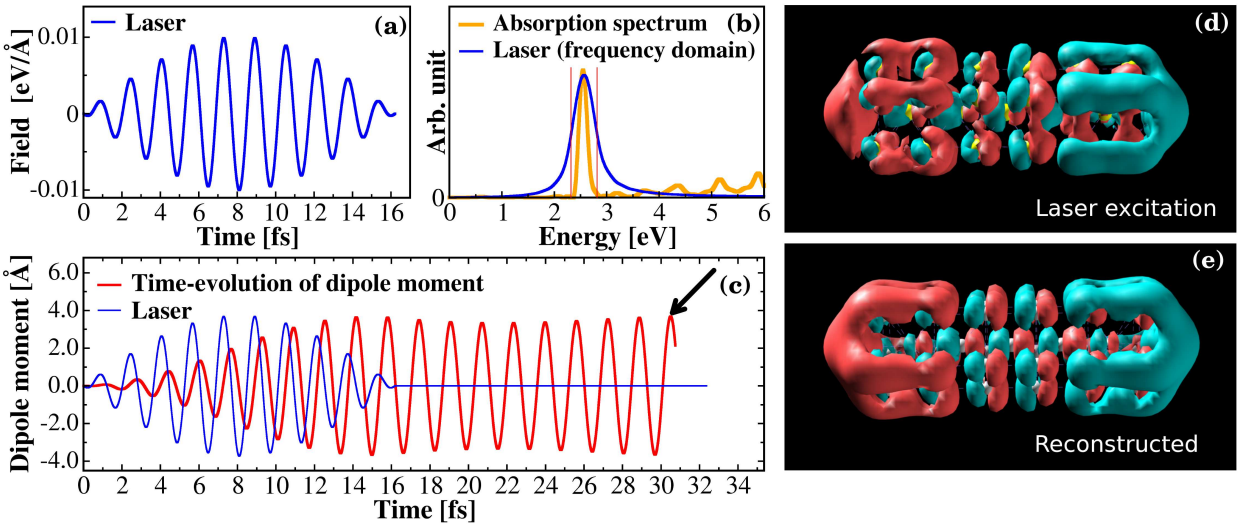

Figure 5: **Quasi-monochromatic laser simulation and Fourier-transform results at LSPR energy of Ag_{37}. (a)** The 2.55 eV quasi-monochromatic laser pulse used to excite the Ag_{37} cluster along its axis. **(b)** The laser pulse in the frequency domain shown along with the absorption spectrum of Ag_{37}. **(c)** The time evolution of the induced dipole moment (shown with the laser pulse in the background for reference). **(d)** The induced density that corresponds to a maximum of the self-sustained oscillating dipole moment, shown by the black arrow in (c). **(e)** Spatial distribution of the mode of the induced density of Ag_{37} reconstructed at $\omega_{sp} = 2.55$eV from the induced density of the $\delta(t)$-kick simulation.

resolved using a much longer propagation time in the δ-kick RT-TDDFT calculation.

In order to validate our approach, in Fig. 5, we compare a snapshot of the reconstructed mode $\mathscr{R}(\mathbf{r}, \omega_{sp}, t)$ from the δ-kick RT-TDDFT simulation with the result from a quasi-monochromatic laser excitation. The time dependence of the laser field is shown in panel (a), and its representation in frequency space is shown in blue in panel (b) along with the absorption spectrum of Ag_{37} (excited along the axis) in orange. Panel (b) demonstrates that the laser field primarily excites the LSPR because only the LSPR falls within the energetic width of the laser pulse. In panel (c), we show in red the time evolution of the dipole moment in the course of and after the excitation. For reference, the blue curve shows again the time dependence of the laser field. The evolution of the dipole moment after the excitation does confirm that the LSPR is dominated by a single excitation. The arrow indicates the moment for which the self-sustained oscillating density is shown in panel (d) to compare with the reconstructed mode $\mathscr{R}(\mathbf{r}, \omega_{sp}, t)$ in panel (e) at $\omega_{sp} = 2.55$eV. This comparison shows that

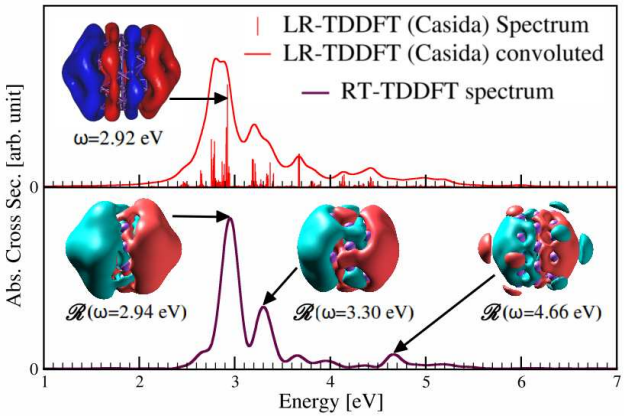

Figure 6: **Absorption spectra of icosahedral Na_{55}^{+}** calculated in RT-TDDFT (lower panel) and LR-TDDFT (upper panel). For the LR-TDDFT calculation, the oscillator strengths are shown both as vertical lines (red) and also as a Lorentzian-convoluted curve (red). The reconstructed modes ($\mathscr{R}(\mathbf{r},\ t = T_i/4, \omega_i)$, where T_i is the period of oscillation) of the electron density oscillation that contribute to the RT-TDDFT induced densities are shown for three different energies in the lower panel. The transition density corresponding to the strongest absorption (at 2.92 eV) as obtained in the LR-TDDFT calculation is shown in the upper panel.

the spatial distributions are equivalent, which corroborates the validity of the reconstruction based on the Fourier transform.

Composite spectral features: Surface modes in simple-metal clusters

As a final test, we analyze the surface modes for the compact icosahedral cluster Na_{55}^{+}, where the charging serves to avoid partial occupations (electronic shell-closing). The lower panel of Fig. 6 shows the RT-TDDFT absorption spectra, whereas the red curve in the upper panel is a convolution of the LR-TDDFT Casida spectrum with a Lorentzian broadening of 0.1 eV. In both the approaches, the spectra are obtained by exciting the cluster along its 5-fold symmetry axis. As before, the RT-TDDFT spectrum is obtained using the code `octopus`, whereas the Casida result is calculted using the code GAUSSIAN. The differences between the two spectra are small and entirely due to technical differences between the `octopus` and

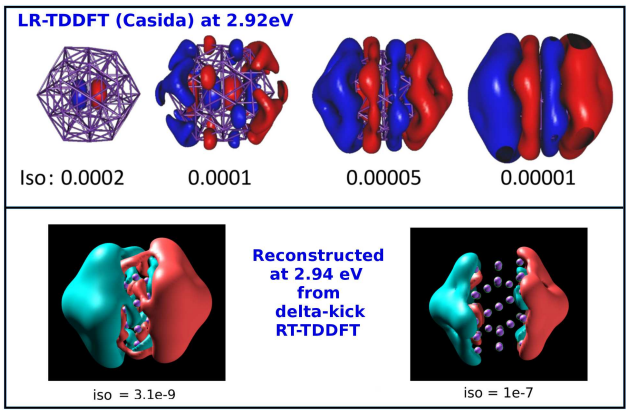

Figure 7: Modes of electron-density oscillation at 2.94 eV in icosahedral Na_{55}^{+}, reconstructed from the induced densities calculated in RT-TDDFT (lower panel), is compared to the transition density obtained from LR-TDDFT (upper panel), at 2.92 eV energy. Different isosurface values are shown in both the cases (RT-TDDFT & LR-TDDFT) to exhibit the distribution of the induced densities in different regions of the cluster.

GAUSSIAN calculations.

First of all, both spectra present a split LSPR with the highest intensity just below 3 eV. The finely-resolved LR-TDDFT spectrum shows that the main contribution comes from an excitation at $\omega = 2.92$ eV. We show its transition density in the upper panel of Fig. 6. The reconstructed modes obtained from the δ-kick RT-TDDFT simulation at the two maxima of the LSPR feature ($\omega = 2.94$ eV and $\omega = 3.30$ eV) are also shown for the same isosurface value in the lower panel of Fig. 6. These two different contributions to the split surface plasmon do not look exactly the same, but they clearly show that the density response of the cluster is primarily from its surface. In perfect agreement with the classical picture,[15] the spatial distribution of the induced density corresponds to an approximate rigid displacement of the density from its equilibrium position, leading to the appearance of the induced density mainly at the surface. For completeness, we have also shown the reconstructed mode at $\omega = 4.66$ eV which, while being a dipole surface mode as well, clearly exhibits a different symmetry. This mode is the so-called *multipole* surface plasmon, which also appears in the optical absorption spectrum of spherical jellium clusters.[24,26]

Focusing on the lower-energy fragment of the LSPR, the snapshots of the sine contribution

to the reconstructed mode at $\omega_{\rm sp} = 2.94$ eV are shown in the lower panel of Fig. 7 for two different isosurface values, confirming the net surface character of the mode. However, the LR-TDDFT transition density at $\omega = 2.92$ eV, shown for different iso-values in the upper panel of Fig. 7, is qualitatively different and cannot be regarded by any means as a surface mode. This mismatch can be traced back to the fact that, unlike the LSPR analyzed in the previous section, the plasmon resonance is now not dominated by a single excitation, but made up by a number of energetically close transtions.[39,60] This can be seen in the LR-TDDFT spectrum in Fig. 6, where there are many closely spaced excitations around the most prominent one just below 3 eV. Thus, unlike in the LR-TDDFT calculation, the RT-TDDFT mode obtained at $\omega_{\rm sp} = 2.94$ eV has significant contributions from excitations in the neighborhood. More specifically, if we neglect the contributions by the non-resonant terms in (13) and (14), the sine coefficient $b(\mathbf{r}, \omega_{\rm sp})$ is the Lorentzian weighted sum of the individual transition densites $c_i(\mathbf{r})$ around $\omega_{\rm sp}$, so the shape of $b(\mathbf{r}, \omega_{\rm sp})$ will be quite robust against small variations of γ and/or $\omega_{\rm sp}$. By contrast, the cosine coefficient will be affected by such small variations, but this does not create problems in the characterization of the absorption properties of the mode. Therefore, whereas the LR-TDDFT transition density will change dramatically if we consider an excitation nearby, the reconstructed RT-TDDFT mode is quite robust.

Due to the composite character of the surface plasmon, the oscillatory mode is actually the driven induced density, that is, the Fourier transform of the δ-kick induced density using a finite damping frequency γ. As a consequence, the RT-TDDFT leads to a more faithful description of the plasmonic response than the LR-TDDFT, since the latter provides the individual contributions $c_j(\mathbf{r})$, but not the driven induced density. Of course, by adding the LR-TDDFT transition densities using (13) and (14) we will recover the plasmon oscillation, as illustrated in the SI for a model jellium Na_{58} cluster. Nonetheless, this is a cumbersone procedure and unapplicable for medium and large clusters. By contrast, if a finer description of the plasmonic response were required, the corresponding information could be extracted

from RT-TDDFT by using a long propagation time. An example can be seen in the SI, where the RT-TDDFT absorption spectrum of the icosahedral Ag_{147}^- cluster is presented with a resolution of 0.018 eV using a propagation time of 250 fs.

Conclusion

We have demonstrated the possibility to accurately extract the modes of electron-density oscillation corresponding to spectral peaks at any energy of interest from a single δ-kick time-evolution / RT-TDDFT calculation. To this end, we Fourier-transform the induced density obtained using a real-space real-time TDDFT code (octopus in our case). We demonstrate the validity of the procedure by comparing with results either from an explicit RT-TDDFT simulation of the excitation process using a monochromatic laser pulse or from linear-response TDDFT calculations in the Casida formalism.

The Fourier-transform reconstructed modes are not only accurate in simple-metal nanostructures. We have also shown that the method can be applied to noble-metal clusters, where it is able to show the intricate interplay between the delocalized metal s electrons and the more strongly localized d electrons. In particular, the dynamical screening of the localized surface-plasmon resonance by the d electrons can be easily visualized using this method.

We have carefully discussed the advantages of the approach when analyzing spectral features that are not dominated by a single excitation, as well as its limits (due to the unavoidable finite spectral resolution of the reconstructed modes). We have shown that the method naturally addresses the composite character of localized surface-plasmon resonances in, e.g., sodium clusters. In particular, the surface character of the driven mode is demonstrated. One only have to keep in mind that the non-absorption dynamics (i.e. the oscillations in phase with the perturbing field) depends in a sensitive manner on the quasi-monochromatic character of the actual perturbative probe.

In conclusion, the Fourier-transform reconstructed modes provide the relevant informa-

tion about the optical spectral features. The present approach is able to overcome the main practical drawback of standard real-time TDDFT calculations, which consists in the unavailability of direct information about the nature of individual electronic excitations that are visible as peaks in optical spectra. It is expected that this method will yet accelerate the implementation and use of the real-time approach in different computational codes.

Availability

A code that carries out the procedure as post-treatment of time-dependent densities calculated using the `octopus` code will be made available shortly.

Acknowledgement

Enlightening discussions with Antonio I. Fernández Domínguez are gratefully acknowledged. We are grateful to Franck Rabilloud for providing us the LR-TDDFT results for Na_{55} as well as for helpful discussions. This work has been carried out thanks to the support of the A*MIDEX grant (n° ANR-11-IDEX-0001-02) funded by the French Government "Investissements d'Avenir" program. We acknowledge support from the French National Research Agency (Agence Nationale de Recherche, ANR) in the frame of the project "FIT SPRINGS", ANR-14-CE08-0009. This work has used HPC resources from GENCI-IDRIS (Grant 2016-096829). PGG acknowledge funding from the Spanish MINECO through the "María de Maeztu" programme for Units of Excellence in R&D (MDM-2014-0377) and through the research grant MAT2014-53432-C5-5-R.

References

(1) Szalay, P. G.; Müller, T.; Gidofalvi, G.; Lischka, H.; Shepard, R. Multiconfiguration Self-Consistent Field and Multireference Configuration Interaction Methods and Ap-

plications. *Chemical Reviews* **2012**, *112*, 108–181, PMID: 22204633.

(2) Helgaker, T.; Jorgensen, P.; Olsen, J. *Molecular Electronic-Structure Theory*; John Willey & Sons, 2014.

(3) Bonacic-Koutecky, V.; Pittner, J.; Boiron, M.; Fantucci, P. An accurate relativistic effective core potential for excited states of Ag atom: An application for studying the absorption spectra of Agn and Agn+ clusters. *The Journal of Chemical Physics* **1999**, *110*, 3876–3886.

(4) Bonacic-Koutecky, V.; Veyret, V.; Mitric, R. Ab initio study of the absorption spectra of Agn (n=5–8) clusters. *The Journal of Chemical Physics* **2001**, *115*, 10450–10460.

(5) Mie, G. Beiträge zur Optik trüber Medien, speziell kolloidaler Metallösungen. *Annalen der Physik* **1908**, *330*, 377–445.

(6) Esteban, R.; Borisov, A. G.; Nordlander, P.; Aizpurua, J. Bridging quantum and classical plasmonics with a quantum-corrected model. *Nature Communications* **2012**, *3*, 825.

(7) Agarwal, G. S.; Pattanayak, D. N.; Wolf, E. Structure of electromagnetic fields in spatially dispersive media of arbitrary geometry. *Phys. Rev. B* **1975**, *11*, 1342–1351.

(8) Ruppin, R. Optical properties of small metal spheres. *Phys. Rev. B* **1975**, *11*, 2871–2876.

(9) Ruppin, R. Plasmon frequencies of small metal spheres. *Journal of Physics and Chemistry of Solids* **1978**, *39*, 233 – 237.

(10) Dasgupta, B. B.; Fuchs, R. Polarizability of a small sphere including nonlocal effects. *Phys. Rev. B* **1981**, *24*, 554–561.

(11) Claro, F.; Fuchs, R. Optical absorption by clusters of small metallic spheres. *Phys. Rev. B* **1986**, *33*, 7956–7960.

(12) Olszewski, S. Long-Wavelength Absorption in Small Metallic Spheres. *physica status solidi (b)* **1993**, *178*, 247–256.

(13) Toscano, G.; Straubel, J.; Kwiatkowski, A.; Rockstuhl, C.; Evers, F.; Xu, H.; Asger Mortensen, N.; Wubs, M. Resonance shifts and spill-out effects in self-consistent hydrodynamic nanoplasmonics. *Nature Communications* **2015**, *6*, 7132.

(14) Runge, E.; Gross, E. K. U. Density-Functional Theory for Time-Dependent Systems. *Physical Review Letters* **1984**, *52*, 997–1000.

(15) Maier, S. A. *Plasmonics: Fundamentals and Applications*; Springer, New York, 2007.

(16) Zhang, P.; Feist, J.; Rubio, A.; García-González, P.; García-Vidal, F. J. Ab initio nanoplasmonics: The impact of atomic structure. *Phys. Rev. B* **2014**, *90*, 161407.

(17) Varas, A.; García-González, P.; García-Vidal, F. J.; Rubio, A. Anisotropy Effects on the Plasmonic Response of Nanoparticle Dimers. *J. Phys. Chem. Lett.* **2015**, *6*, 1891–1898.

(18) Barbry, M.; Koval, P.; Marchesin, F.; Esteban, R.; Borisov, A. G.; Aizpurua, J.; Sánchez-Portal, D. Atomistic Near-Field Nanoplasmonics: Reaching Atomic-Scale Resolution in Nanooptics. *Nano Lett.* **2015**, *15*, 3410–3419.

(19) Rossi, T. P.; Zugarramurdi, A.; Puska, M. J.; Nieminen, R. M. Quantized Evolution of the Plasmonic Response in a Stretched Nanorod. *Phys. Rev. Lett.* **2015**, *115*, 236804.

(20) Weissker, H.-C.; Lopez-Lozano, X. Surface plasmons in quantum-sized noble-metal clusters: TDDFT quantum calculations and the classical picture of charge oscillations. *Phys. Chem. Chem. Phys.* **2015**, *17*, 28379–28386.

(21) Kuisma, M.; Sakko, A.; Rossi, T. P.; Larsen, A. H.; Enkovaara, J.; Lehtovaara, L.; Rantala, T. T. Localized surface plasmon resonance in silver nanoparticles: Atomistic first-principles time-dependent density-functional theory calculations. *Phys. Rev. B* **2015**, *91*, 115431.

(22) Marchesin, F.; Koval, P.; Barbry, M.; Aizpurua, J.; Sánchez-Portal, D. Plasmonic Response of Metallic Nanojunctions Driven by Single Atom Motion: Quantum Transport Revealed in Optics. *ACS Photonics* **2016**, *3*, 269–277.

(23) Urbieta, M.; Barbry, M.; Zhang, Y.; Koval, P.; Sánchez-Portal, D.; Zabala, N.; Aizpurua, J. Atomic-Scale Lightning Rod Effect in Plasmonic Picocavities: A Classical View to a Quantum Effect. *ACS Nano* **2018**, *12*, 585–595.

(24) Ekardt, W. Dynamical Polarizability of Small Metal Particles: Self-Consistent Spherical Jellium Background Model. *Phys. Rev. Lett.* **1984**, *52*, 1925–1928.

(25) Brack, M. The physics of simple metal clusters: self-consistent jellium model and semiclassical approaches. *Rev. Mod. Phys.* **1993**, *65*, 677–732.

(26) Varas, A.; García-González, P.; Feist, J.; García-Vidal, F. J.; Rubio, A. Quantum plasmonics: from jellium models to ab initio calculations. *Nanophotonics* **2016**, *5*, 409–426.

(27) Rabilloud, F. Assessment of the Performance of Long-Range-Corrected Density Functionals for Calculating the Absorption Spectra of Silver Clusters. *The Journal of Physical Chemistry A* **2013**, *117*, 4267–4278, PMID: 23638637.

(28) Rabilloud, F. Description of plasmon-like band in silver clusters: The importance of the long-range Hartree-Fock exchange in time-dependent density-functional theory simulations. *The Journal of Chemical Physics* **2014**, *141*, 144302.

(29) Jin, R.; Zeng, C.; Zhou, M.; Chen, Y. Atomically Precise Colloidal Metal Nanoclusters and Nanoparticles: Fundamentals and Opportunities. *Chemical Reviews* **2016**, *116*, 10346–10413, PMID: 27585252.

(30) Weissker, H.-C.; Escobar, H. B.; Thanthirige, V. D.; Kwak, K.; Lee, D.; Ramakrishna, G.; Whetten, R.; ; López-Lozano, X. Information on quantum states pervades

the visible spectrum of the ubiquitous Au144 gold nanocluster. *Nature Communications* **2014**, *5*, 3785.

(31) Weissker, H.-C.; Lopez-Acevedo, O.; Whetten, R. L.; López-Lozano, X. Optical Spectra of the Special Au144 Gold-Cluster Compounds: Sensitivity to Structure and Symmetry. *The Journal of Physical Chemistry C* **2015**, *119*, 11250–11259.

(32) Lopez-Lozano, X.; Plascencia-Villa, G.; Calero, G.; Whetten, R. L.; Weissker, H.-C. Is the largest aqueous gold cluster a superatom complex? Electronic structure & optical response of the structurally determined Au146(p-MBA)57. *Nanoscale* **2017**, *9*, 18629–18634.

(33) Malola, S.; Lehtovaara, L.; Enkovaara, J.; Häkkinen, H. Birth of the Localized Surface Plasmon Resonance in Monolayer-Protected Gold Nanoclusters. *ACS Nano* **2013**, *7*, 10263–10270.

(34) Barcaro, G.; Sementa, L.; Fortunelli, A.; Stener, M. Comment on "(Au-Ag)144(SR)60 alloy nanomolecules" by C. Kumara and A. Dass, Nanoscale, 2011, 3, 3064. *Nanoscale* **2014**..

(35) Casida, M. E. *In Recent Developments and Applications of Modern Density Functional Theory (ed. J. M. Seminario)*; Elsevier, Amsterdam, 1996; Vol. 4.

(36) Kohn, W.; Sham, L. J. Self-Consistent Equations Including Exchange and Correlation Effects. *Phys. Rev.* **1965**, *140*, A1133–A1138.

(37) Yabana, K.; Bertsch, G. F. Time-dependent local-density approximation in real time. *Phys. Rev. B* **1996**, *54*, 4484–4487.

(38) Yabana, K.; Nakatsukasa, T.; Iwata, J.-I.; Bertsch, G. F. Real-time, real-space implementation of the linear response time-dependent density-functional theory. *physica status solidi (b)* **2006**, *243*, 1121–1138.

(39) Townsend, E.; Bryant, G. W. Plasmonic Properties of Metallic Nanoparticles: The Effects of Size Quantization. *Nano Letters* **2012**, *12*, 429–434, PMID: 22181554.

(40) Rossi, T. P.; Kuisma, M.; Puska, M. J.; Nieminen, R. M.; Erhart, P. Kohn–Sham Decomposition in Real-Time Time-Dependent Density-Functional Theory: An Efficient Tool for Analyzing Plasmonic Excitations. *Journal of Chemical Theory and Computation* **2017**, *13*, 4779–4790, PMID: 28862851.

(41) Weissker, H.-C.; Lopez-Lozano, X. Surface plasmons in quantum-sized noble-metal clusters: TDDFT quantum calculations and the classical picture of charge oscillations. *Phys. Chem. Chem. Phys.* **2015**, *17*, 28379–28386.

(42) Weissker, H.-C.; Whetten, R. L.; López-Lozano, X. Optical response of quantum-sized Ag and Au clusters - cage vs. compact structures and the remarkable insensitivity to compression. *Phys. Chem. Chem. Phys.* **2014**, *16*, 12495–12502.

(43) López-Lozano, X.; Barron, H.; Mottet, C.; Weissker, H.-C. Aspect-ratio and size-dependent emergence of the surface-plasmon resonance in gold nanorods - an ab initio TDDFT study. *Phys. Chem. Chem. Phys.* **2014**, *16*, 1820–1823.

(44) Sinha-Roy, R.; García-González, P.; Weissker, H.-C.; Rabilloud, F.; Fernández-Domínguez, A. I. Classical and ab Initio Plasmonics Meet at Sub-nanometric Noble Metal Rods. *ACS Photonics* **2017**, *4*, 1484–1493.

(45) Sinha-Roy, R.; López-Lózano, X.; Whetten, R. L.; García-González, P.; Weissker, H.-C. In Search of the Quantum-Electronic Origin of Color Change: Elucidation of the Subtle Effects of Alloying with Copper on ≈1.8 nm Gold Nanoclusters. *The Journal of Physical Chemistry C* **2017**, *121*, 5753–5760.

(46) Gao, S. Nonlinear response of metal nanoparticles: Double plasmon excitation and electron transfer. *The Journal of Chemical Physics* **2015**, *142*, 234701.

(47) Wang, B.-J.; Xu, Y.; Ke, S.-H. Plasmon excitations in sodium atomic planes: A time-dependent density functional theory study. *The Journal of Chemical Physics* **2012**, *137*, 054101.

(48) Xiang, H.; Zhang, X.; Neuhauser, D.; Lu, G. Size-Dependent Plasmonic Resonances from Large-Scale Quantum Simulations. *The Journal of Physical Chemistry Letters* **2014**, *5*, 1163–1169, PMID: 26274465.

(49) Marques, M. A.; Castro, A.; Bertsch, G. F.; Rubio, A. octopus a first-principles tool for excited electron-ion dynamics. *Computer Physics Communications* **2003**, *151*, 60 – 78.

(50) Castro, A.; Appel, H.; Oliveira, M.; Rozzi, C. A.; Andrade, X.; Lorenzen, F.; Marques, M. A. L.; Gross, E. K. U.; Rubio, A. octopus: a tool for the application of time-dependent density functional theory. *physica status solidi (b)* **2006**, *243*, 2465–2488.

(51) Andrade, X.; Strubbe, D.; De Giovannini, U.; Larsen, A. H.; Oliveira, M.; Alberdi-Rodriguez, J.; Varas, A.; Theophilou, I.; Helbig, N.; Verstreate, M. et al. Real-space grids and the Octopus code as tools for the development of new simulation approaches for electronic systems. *Phys. Chem. Chem. Phys.* **2015**, *17*, 31371–31396.

(52) Troullier, N.; Martins, J. L. Efficient pseudopotentials for plane-wave calculations. *Phys. Rev. B* **1991**, *43*, 1993–2006.

(53) Perdew, J. P.; Burke, K.; Ernzerhof, M. Generalized Gradient Approximation Made Simple. *Phys. Rev. Lett.* **1996**, *77*, 3865–3868.

(54) Bernadotte, S.; Evers, F.; Jacob, C. R. Plasmons in molecules. *J. Phys. Chem. C* **2013**, *117*, 1863–1878.

(55) Johnson, H. E.; Aikens, C. M. Electronic Structure and TDDFT Optical Absorption Spectra of Silver Nanorods. *The Journal of Physical Chemistry A* **2009**, *113*, 4445–4450.

(56) Guidez, E. B.; Aikens, C. M. Diameter Dependence of the Excitation Spectra of Silver and Gold Nanorods. *The Journal of Physical Chemistry C* **2013**, *117*, 12325–12336.

(57) Taylor, K.; Pettiette-Hall, C.; Cheshnovsky, O.; Smalley, R. Ultraviolet photoelectron spectra of coinage metal clusters. *J. Chemical Physics* **1992**, *96*, 3319.

(58) Liebsch, A. Surface-plasmon dispersion and size dependence of Mie resonance: Silver versus simple metals. *Phys. Rev. B* **1993**, *48*, 11317–11328.

(59) Cottancin, E.; Celep, G.; Lermé, J.; Pellarin, M.; Huntzinger, J.; Vialle, J.; Broyer, M. Optical Properties of Noble Metal Clusters as a Function of the Size: Comparison between Experiments and a Semi-Quantal Theory. *Theoretical Chemistry Accounts: Theory, Computation, and Modeling (Theoretica Chimica Acta)* **2006**, *116*, 514.

(60) Yannouleas, C.; Vigezzi, E.; Broglia, R. A. Evolution of the optical properties of alkali-metal microclusters towards the bulk: The matrix random-phase-approximation description. *Phys. Rev. B* **1993**, *47*, 9849–9861.

Graphical TOC Entry